CORPUS PUBLISHERS

Journal of Mineral and Material Science (JMMS)

ISSN: 2833-3616

Volume 6 Issue 3, 2025

Article Information

Received date : April 06, 2025

Published date: May 05, 2025

*Corresponding author

Freddy H Escobar, Petroleum Engineering Department, Universidad Surcolombiana, Colombia

DOI: 10.54026/JMMS/1116

Key Words

Transient Pressure Analysis; Tiab's Direct Synthesis (TDS); Shale Reservoirs; Multi-Fractured Horizontal Wells (MFHWs); Five-Region Flow Model; Pressure-Dependent Permeability

Review Article

Transient Flow Modeling in Shale Reservoirs Using TDS Technique and a Five-Zone Framework

Freddy H Escobar*, Nathaly Perdomo-Rojas and Camila Lozano-Rojas

Universidad Surcolombiana, Petroleum Engineering Department, Colombia

Abstract

This study presents an extension of the Tiab's Direct Synthesis (TDS) technique to Multi-Fractured Horizontal Wells (MFHWs) in shale formations, using a five-region analytical model. The model accounts for pressure-dependent rock and fluid properties and incorporates multiple linear flow regimes to represent the complex interaction between the matrix and fractures. Using dimensionless analysis, a set of analytical expressions was derived to estimate key reservoir parameters such as half-fracture length, reservoir length, and effective permeability. The methodology also identifies critical flow regimes and transition points-early linear flow, intermediate pseudosteady-state, transitional linear flow, and late-time pseudosteady-state-through characteristic slopes and curve intersections in pressure and reciprocal rate derivatives.

Although a wide range of permeability and geometric variations were evaluated, two synthetic examples are presented to validate the methodology. The estimated parameters closely matched the input values, with relative errors below 2%, confirming the accuracy of the proposed approach. Despite the robustness of the methodology, the dimensionless permeability modulus showed inconsistent unification across all cases, indicating an area for future refinement. Overall, the extended TDS technique offers a reliable, practical, and theoretically sound framework for interpreting transient tests in unconventional shale reservoirs with MFHWs. Also, equations are presented for the application of straight-line conventional analysis.

Introduction

Shale formations, due to their ultra-low permeability and complex geological structure, present unique challenges for reservoir characterization and development. Traditionally, pressure tests and transient flow rate analysis have been employed for reservoir evaluation-methods that have proven effective in more conventional, higher-permeability formations. However, the specific characteristics of shale-such as nonlinear flow behavior and limited pore connectivity-demand more advanced and tailored analytical approaches [1]. The advent of hydraulically fractured Multi-Fractured Horizontal Wells (MFHWs) has revolutionized shale exploitation by increasing reservoir contact and enabling more efficient hydrocarbon production. Nonetheless, interpreting pressure and reciprocal rate tests in such wells remains a challenge due to the added complexity of multiple fractures and the presence of multiphase flow [2]. Conventional analytical methods, which perform well in homogeneous and high-permeability settings, are inadequate for MFHW systems. These techniques often fail to capture the combined effects of hydraulic fracturing and the ultra-low permeability of shale matrices, leading to unreliable or oversimplified interpretations. Furthermore, traditional straight-line diagnostic methods lack the robustness needed to handle the flow complexity inherent in multi fractured shale systems. This underscores the urgent need for improved analytical methodologies capable of providing accurate and reliable characterization of these unconventional reservoirs.

Currently, there is a notable gap in the availability of dedicated analytical techniques that can effectively characterize shale formations using pressure and reciprocal rate testing in MFHWs. Ongoing efforts have aimed to enhance linear flow models to improve their predictive capacity, particularly regarding bottomhole pressure behavior and reservoir depletion time in shale gas and tight formations, including advancements to the classic trilinear flow model [2]. These types of reservoirs often exhibit strong coupling between pore pressure and permeability variations, further motivating model refinement [1].

The five-region model is an extension of the traditional trilinear flow concept, in which the reservoir is divided into five distinct zones rather than three. This approach is specifically adapted to simulate the complex behavior of unconventional systems with MFHWs [3]. It simplifies fluid flow dynamics by modeling them as a sequence of interconnected linear flow regimes [2]. Earlier applications of linear flow models in multiphase hydraulic fracturing, especially in shale formations with high liquid content, were typically restricted to classical solutions based on the diffusivity equation. The five-region model introduces a more flexible analytical framework, incorporating pressure-dependent rock and fluid properties, thereby extending its applicability to a broader range of multiphase flow conditions [3]. Liquid extraction in shale reservoirs with high hydrocarbon content and ultra-low permeability requires significantly larger pressure drops than in conventional systems. Under these conditions, rock and fluid properties are highly sensitive to pressure, rendering constant-property assumptions invalid [4]. The modified five-region model (Figure 1) introduces Region 2, representing the Stimulated Reservoir Volume (SRV), which exhibits enhanced permeability due to fracture branching induced by hydraulic stimulation. In contrast, Regions 3, 4, and 5 represent the original matrix, which retains its native properties (Figure 2). The model accounts for unaltered rock matrix zones between fractures, making it particularly suitable for simulating MFHWs with limited fracture extension [2].

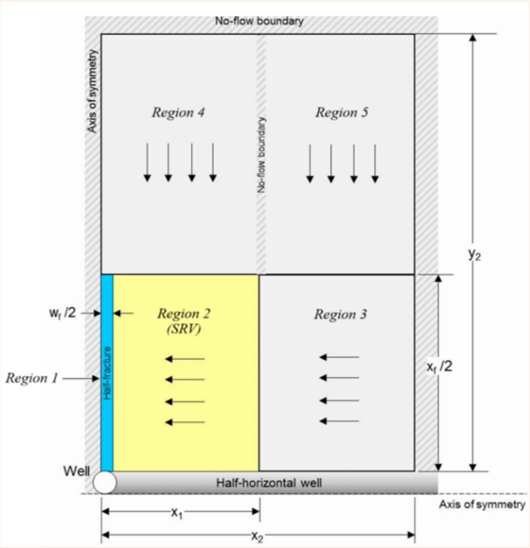

Figure 1: Five-region reservoir domain, after [4].

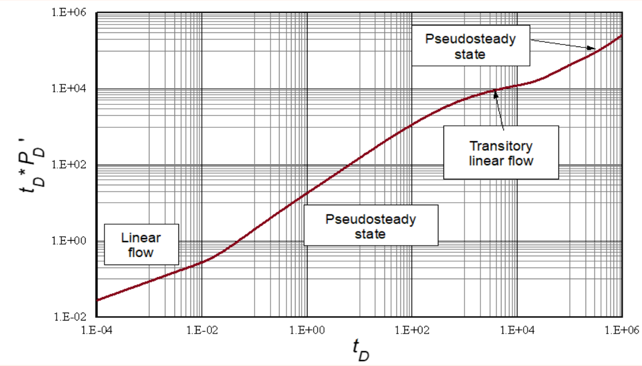

Figure 2: Observed flow regimes with $\gamma_D = 0$.

In practice, fractures in MFHWs frequently exhibit branching patterns rather than idealized bi-wing geometries. This branching forms high-permeability zones around each fracture, significantly impacting production performance. Even in tight formations, the unstimulated surrounding matrix can make substantial contributions to long-term production [3]. The five-region model has thus become a valuable tool for estimating critical properties such as SRV permeability and fracture conductivity [2]. It is capable of simulating systems where fractures are surrounded by localized SRVs, while the rest of the reservoir remains unstimulated. The model also incorporates flow in the surrounding unfractured region, both parallel and perpendicular to the fractures [3]. The model proposed by Molina OM [2,4] distinguishes itself by eliminating the need for pseudo functions, commonly used in conventional models. Instead, it incorporates exponential formulations to describe the relationships between pressure and fluid/rock properties, leveraging the proven utility of exponential functions for modeling pressure-sensitive behavior. As a result, the five-region model offers a versatile, accurate, and user-friendly analytical framework. It is particularly suitable for predicting multiphase flow behavior in pressure-sensitive environments, especially under high-pressure gradient conditions [4].

Tiab [5] introduced the Tiab's Direct Synthesis (TDS) Technique as a practical, precise, and revolutionary approach for well test interpretation. This methodology uses characteristic points and lines on pressure and pressure derivative log-log plots for direct parameter estimation. The technique has since been extended to shale formations by Bernal KM, et al. [6-9]. The present study applies the five-region model developed by Molina O, et al. [4] to generate transient pressure and rate data in order to extend the TDS Technique to MFHWs in shale reservoirs. The derived expressions were validated using synthetic data and demonstrated excellent accuracy.

Transient Pressure Behavior

The mathematical model used in this work was presented by Molina O & Zeidouni [4] and considers a five-region domain as depicted in Figure 1 along the reservoir's dimensions and it included pressure-sensitive effects as given by Pedrosa [10], who introduced the permeability modulus:

$$\gamma = \frac{1}{k}\left(\frac{\partial k}{\partial P}\right) \quad (1)$$

which dimensionless quantity is given by:

$$\gamma_D = \frac{141.2 q \mu B}{k_i h}\gamma \quad (2)$$

The dimensionless pressure derivative versus dimensionless time log-log plot obtained with the model of [4] which is based upon the flow domain given in Figure 1. From left to right, as time increases, the following features are observed there:

Early linear flow regime: During this stage, fluid flows from the fractures closest to the wellbore, which dominates the early-time behavior due to their high permeability. The flow is predominantly One-Dimensional (1D), resulting in a linear flow pattern represented by a 0.5 slope on the dimensionless pressure derivative curve. As pressure declines within the fractures, fluid stored in the matrix gradually transfers into the fractures before reaching the wellbore. The high fracture permeability enables rapid initial production, though it may also lead to accelerated local depletion.

Intermediate pseudosteady state period: Following the linear flow regime, the system may transition into an early pseudosteady state, suggesting that the fractured region has been significantly drained and begins to behave as a more stable system. Pressure declines more uniformly across the system, and the pressure response exhibits a slope of 1 on the log-log plot, characteristic of pseudosteady-state flow. At this point, the well is surrounded by a high-permeability zone, where a temporary equilibrium can be established before the broader reservoir begins to respond.

Transitional linear flow: A return to transient behavior suggests that the well has started draining beyond the fractured or high-permeability zone and is now influencing a new portion of the reservoir. This indicates the system is no longer in equilibrium, and pressure begins to respond dynamically once again. If the initial high-permeability region is depleted, this transient flow reflects the outward expansion of the drainage front into a lower-permeability matrix. In rate transient tests a slope of 0.3 is seen instead of the transitional linear regime which may be due to a fractal flow taking place.

Late-time pseudosteady state period: The second appearance of a pseudosteady state implies that the system has reached a new drainage equilibrium, now on a larger scale. At this point, flow has stabilized at the level of the entire reservoir, with pressure declining at a constant rate throughout the system. This indicates that the well, after depleting the high-permeability zone, is now influencing the rest of the reservoir, and this late-time pseudosteady state reflects the large-scale behavior of the field.

Dimensionless permeability modulus: In certain reservoirs, particularly fractured and low-permeability formations like the one under study, a delayed effect associated with the permeability modulus may appear at the end of the pressure test. This effect is evidenced by a change in the slope of the pressure curve during late-time behavior, indicating that the system's permeability is not constant but pressure-dependent. Possible causes of this phenomenon include matrix compaction or progressive fracture closure. Such behavior can negatively impact long-term production, as a gradual reduction in reservoir connectivity will lead to reduced productivity. Both linear and pseudosteady-state flow regimes are essential for a comprehensive understanding of reservoir behavior. While linear flow provides critical insights during the early stages of production or in reservoirs with well-defined geometries, the pseudosteady-state flow regime is crucial for evaluating long-term reservoir performance and forecasting future production.

In practice, reservoir engineers rely on numerical simulations and analytical models to interpret pressure and production test data across both flow regimes. These tools enable the identification of transitions between flow regimes, the calibration of reservoir behavior models, and the optimization of production strategies aimed at maximizing hydrocarbon recovery. A deep understanding of linear and pseudosteady-state flow regimes is not only vital for accurate reservoir data interpretation, but also for informed strategic decision-making in oil and gas resource management. With advances in technology and the continuous improvement of simulation models, the analysis of these flow regimes is expected to evolve further, offering increasingly detailed and accurate insights into reservoir behavior.

TDS Technique for Transient Pressure Analysis

The expressions for dimensionless time, pressure, pressure derivative, reciprocal rate, and reciprocal rate derivative are as follows:

$$t_D = \frac{0.0002637kt}{\phi \mu c_t x_f^2} \quad (3)$$

$$P_D = \frac{kh}{141.2q\mu B} \Delta P \quad (4)$$

$$t_D * P_D' = \frac{k_1 h(t*\Delta P')}{141.2q\mu B} \quad (5)$$

$$\frac{1}{q_D} = \frac{kh\Delta P}{141.2\mu B}\frac{1}{q} \quad (6)$$

$$[t_D * (1/q_D)'] = \frac{kh\Delta P}{141.2\mu B}[t * (1/q)'] \quad (7)$$

Figure 3 illustrates the pressure derivative behavior for various inner reservoir permeability values. Changes in permeability influence both the early and intermediate linear flow regimes. A unified response of the early linear flow regime is presented in Figure 4.

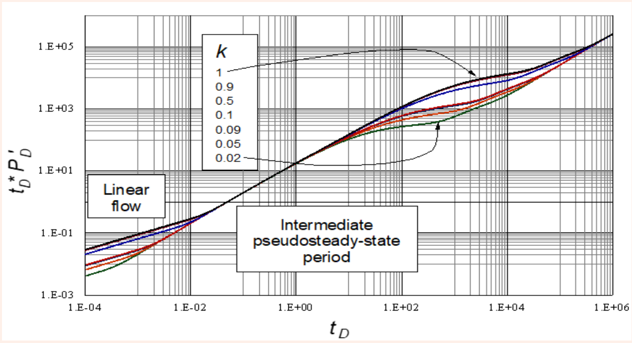

Figure 3: Pressure derivative behavior for different permeability values.

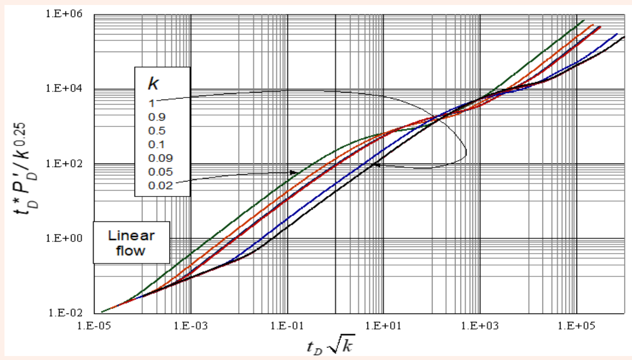

Figure 4: Unified early linear flow regime for different permeability values.

The early-time linear flow regime in Figure 4 is described by the following linear equation:

$$(t_D * P_D')_{EL} k^{-0.25} = 6.5088\sqrt{(t_D)_{EL} k^{0.5}} \quad (8)$$

By substituting the dimensionless quantities from Equations (3) and (5) into Equation (8), permeability is eliminated, resulting in the following expression:

$$x_f = \sqrt{\frac{42.3645q^2B^2\mu t_{EL}}{h^2(t*\Delta P')_{EL}^2 \phi c_t}} \quad (9)$$

Returning to Figure 3, the plot of dimensionless pressure derivative versus dimensionless time exhibits a uniform trend during the intermediate pseudosteady-state period. Consequently, no additional manipulation is necessary in this case, as this period conforms to the following governing equation:

$$(t_D * P_D')_{IP} = 0.6434(t_D)_{IP} \quad (10)$$

Substituting the dimensionless pressure derivative and dimensionless time expressions from Equations (5) and (3), respectively, and solving for the half-fracture length yields the following expression:

$$x_f = \sqrt{\frac{0.6434qBt_{IP}}{\phi c_t h(t*\Delta P')_{IP}}} \quad (11)$$

Figure 5 presents a log-log plot of the dimensionless pressure derivative normalized by permeability raised to the 0.6 power, plotted against dimensionless time. The governing equation describing this linear flow regime is provided below:

$$(t_D * P_D')_{TL} k^{-0.6} = 329.1775\sqrt{(t_D)_{TL}} \quad (12)$$

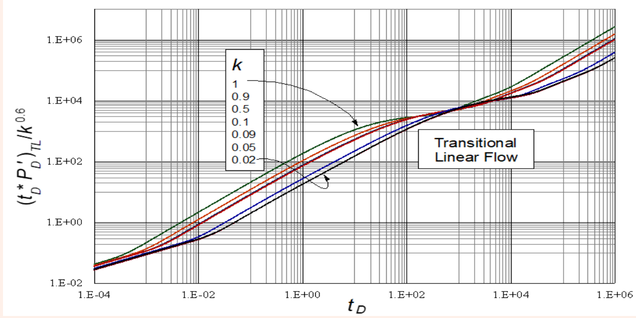

Figure 5: Unified transitory linear flow regime for different permeability values.

Again, replacing the dimensionless quantities into Equation (12) provides:

$$k = \left(\frac{\phi\mu c_t h^2 (t*\Delta P')_{TL}}{1083557.82q^2\mu^2B^2t_{TL}}\right)^5 \quad (13)$$

The intersection point between the early linear flow regime and the intermediate pseudosteady-state period (t_{ELIPi}), obtained by equating Equations (8) and (10), yields the following expression:

$$0.6434(t_D)_{ELIPi} k^{-0.25} = 6.5088\sqrt{(t_D)_{ELIPi} k^{0.5}} \quad (14)$$

Upon solving for the half-fracture length at the intersection point, the resulting expression is as follows:

$$x_f = \sqrt{\frac{0.4140t_{ELIPi}}{42.3645\phi\mu c_t}} \quad (15)$$

Additionally, the intersection point between the intermediate linear flow regime and the preceding intermediate pseudosteady-state period-denoted as t_{IPTLi} - is determined by equating Equations (10) and (12), leading to the following expression:

$$0.6434(t_D)_{IPTLi} k^{-0.6} = 329.1715\sqrt{(t_D)_{IPITi}} \quad (16)$$

$$k = \left(\frac{t_{IPTLi}}{261736.43\phi\mu c_t x_f^2}\right)^5 \quad (17)$$

Figure 6 displays the influence of the dimensionless permeability modulus on the pressure derivative response. Due to the absence of a consistent behavior over the full range of permeability moduli, a separation approach was adopted. Based on Figure 7, the dimensionless time at which the vertical trend occurs is identified as:

$$(t_D\gamma_D^{1.2})_v = 0.0212(t_D\gamma_D^{1.2})_v = 0.0212 \quad (18)$$

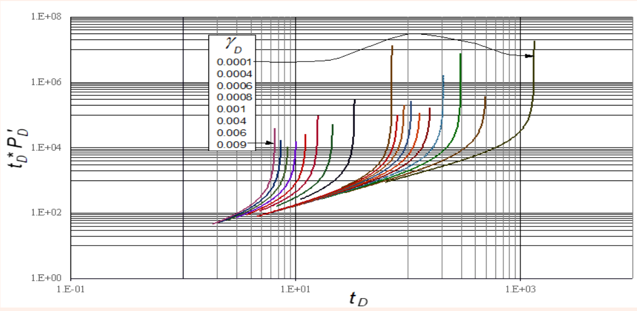

Figure 6: Dimensionless pressure derivative versus dimensionless time behavior for different dimensionless permeability moduli.

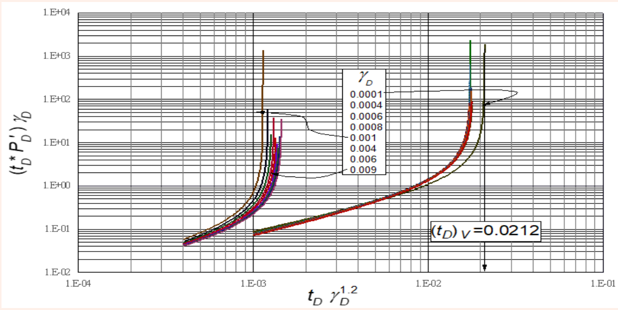

Figure 7: Unified pressure derivative behavior for different dimensionless permeability moduli.

Substituting the dimensionless time from Equation (3) into Equation (18) and solving for the dimensionless permeability modulus yields the following expression:

$$\gamma_D = 193.494\left(\frac{\phi\mu c_t x_f^2}{k t_v}\right)^{1.2} \quad (19)$$

The influence of the length of the second region (refer to Figure 1) is illustrated in Figure 8. A unified behavior for this case is presented in Figure 9, from which the following governing expression is derived for the transitional linear flow regime. Thus:

$$[(t_D * P_D')_{TL} x_1] = 5489.57\left(\sqrt{(t_D)_{TL} x_1}\right) \quad (20)$$

Solving the resulting expression for the length of the second region, X_1, yields:

$$x_1 = \frac{30135435 q^2 \mu B^2 t_{TL}}{\phi c_t x_f^2 k h^2 (t*\Delta P')^2_{TL}} \quad (21)$$

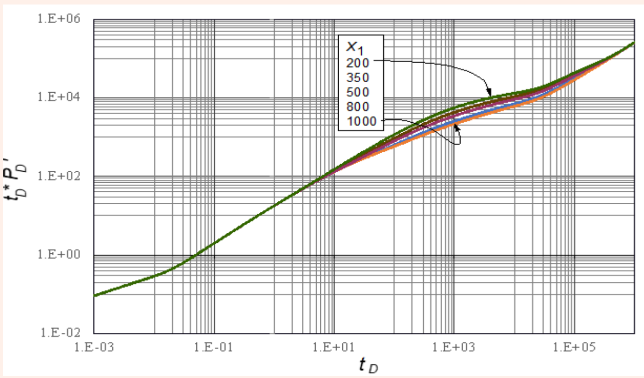

Figure 8: Dimensionless pressure derivative versus dimensionless time behavior for different region-2-length, X_1.

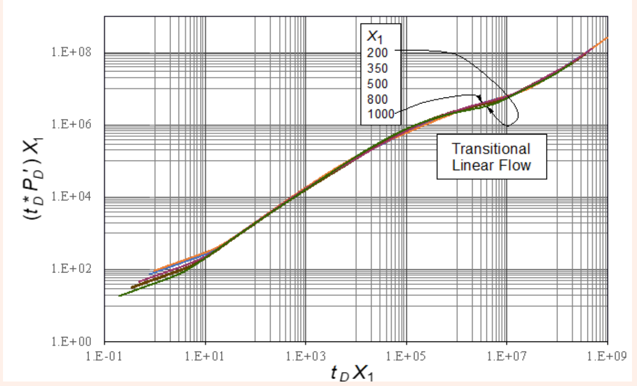

Figure 9: Unified dimensionless pressure derivative versus dimensionless time behavior for different region-2-length, X_1.

As expected, the late-time pseudosteady-state behavior is influenced by the reservoir size (width). Figure 10 presents the pressure derivative response for various reservoir widths, y_2. A unified trend for the late-time pseudosteady-state regime is observed in Figure 11, from which the following relationship is derived:

$$(t_D * P_D')_{LP} = 39.51\frac{(t_D)_{LP}}{y_2} \quad (22)$$

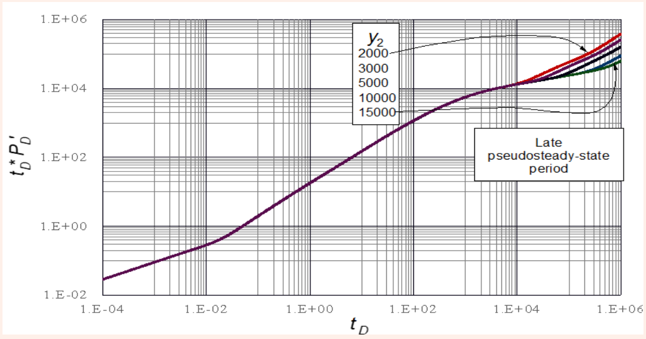

Figure 10: Impact of the total reservoir with, y_2, on the late time of the dimensionless pressure derivative versus dimensionless time.

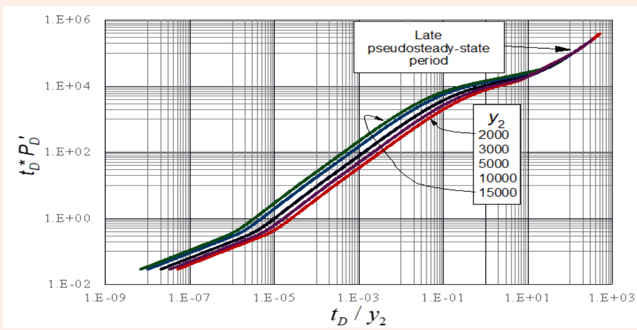

Figure 11: Unified late time pseudosteady-state period for different y_2 values.

By substituting the dimensionless parameters from Equations (3) and (5) and solving for the reservoir width y_2, the following expression is obtained:

$$y_2 = \frac{39.51 q B t_{LP}}{\phi c_t x_f^2 h (t*\Delta P')_{LP}} \quad (23)$$

The intersection of the early linear flow line (Equation 8) and the intermediate linear flow regime line (Equation 10) with the late-time pseudosteady-state line (Equation 22) yields the following intersection points:

$$6.5088k^{0.25}\sqrt{(t_D)_{ELLPi}}\,k^{0.5} = 39.51\frac{(t_D)_{ELLPi}}{y_2} \quad (24)$$

$$329.1775k^{0.6}\sqrt{(t_D)_{TLLPi}} = 39.51\frac{(t_D)_{TLLPi}}{y_2} \quad (25)$$

Solving Equation (24) for reservoir width and Equation (25) for permeability yields the following expressions:

$$y_2 = \frac{1}{10.1447x_f}\sqrt{\frac{t_{ELLPi}}{\phi\mu c_t}} \quad (26)$$

$$k = \left(\frac{1}{513.06x_f y_2}\sqrt{\frac{t_{TLLPi}}{\phi\mu c_t}}\right)^{10} \quad (27)$$

TDS Technique for Transient Rate Analysis

Based on the plot of the reciprocal flow rate derivative $[t_D*(1/q_D)']$, provided in Figure 12, the following flow regimes can be identified:

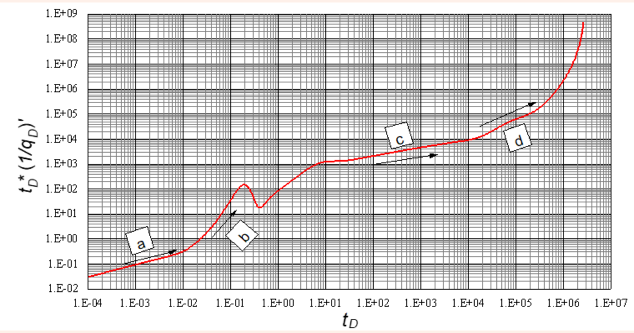

Figure 12: Dimensionless reciprocal rate derivative versus dimensionless time for the five-region model provided by Molina O & Zeidouni [4].

(a): An early linear flow regime is observed, characterized by a 0.5 slope on the log-log scale. At this stage, the reservoir matrix has not yet begun to release fluid significantly; flow is dominated by the highly permeable fractures.

(b): This is a transitional zone where interaction with the matrix begins. Although fluid starts moving from the matrix to the fractures, it is not yet sufficient to dominate the system. Flow is no longer purely linear within the fractures.

(c): This zone shows a non-distinctive or undefined behavior, possibly due to complex flow mechanisms (fractal domain). Such responses are typically observed in naturally fractured reservoirs with low matrix permeability, where fluid is released from the matrix very slowly.

(d): This stage corresponds to a pseudosteady-state flow period, reflecting a dynamic equilibrium between the matrix and fractures. The rate of fluid transfer from the matrix to the fractures becomes approximately constant, indicating a stabilized contribution from the system.

Finally, the plot shows a late-time upward trend, which suggests the onset of reservoir boundary effects. At this point, pressure begins to decline more rapidly, potentially marking the start of production decline. This behavior may call for stimulation strategies such as additional fracturing or fluid injection to sustain productivity.

In summary, the evolution of the transient flow behavior clearly reflects the interaction between matrix and fractures: initially dominated by fractures (linear flow), followed by a transitional phase with increasing matrix contribution, then reaching a dynamic equilibrium (pseudosteady-state flow), and finally entering a phase where boundary effects lead to sharp pressure and production declines.

The influence of permeability on the pressure derivative, analogous to that in pressure transient analysis, is shown in Figure 13. A unified trend is observed in Figure 14, from which the following expressions were obtained:

$$[t_D*(1/q_D)']_{EL}k = 6.299\sqrt{(t_D)_{EL}k^{-1}} \quad (28)$$

$$[t_D*(1/q_D)']_{IP}k = 0.0278(t_D/k)_{IP} \quad (29)$$

$$[t_D*(1/q_D)']_{UF}k = 5913.62[(t_D)_{UF}/k]^{0.3} \quad (30)$$

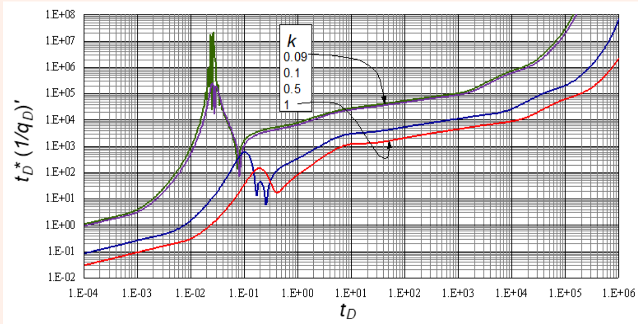

Figure 13: Effect of the permeability on the dimensionless reciprocal rate derivative versus dimensionless time.

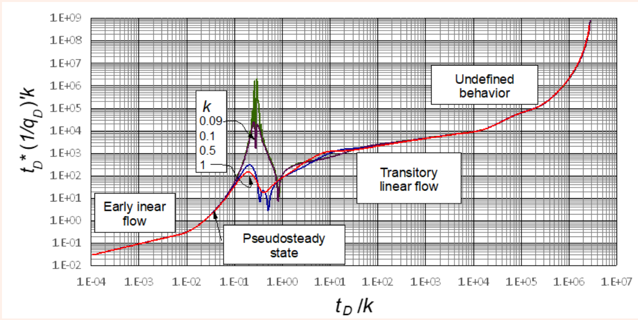

Figure 14: Unified behavior of the dimensionless reciprocal rate derivative versus dimensionless time under permeability changes.

Once again, by substituting the dimensionless quantities defined in Equations (3) and (7) into Equations (28), (29), and (30), and solving for reservoir permeability, the following expressions are respectively obtained:

$$k = \sqrt[4]{\frac{39.69\mu B^2 t_{EL}}{\phi c_t x_f^2 h^2 \Delta P^2 [t*(1/q)']_{EL}^2}} \quad (31)$$

$$k = \sqrt{\frac{0.0278Bt_{IP}}{\phi c_t x_f^2 h\Delta P\,[t*(1/q)']_{IP}}} \quad (32)$$

$$k = \sqrt{\frac{5913.62\mu B t_{UF}^{0.3}}{(\phi\mu c_t x_f^2)^{0.3} h\Delta P[t*(1/q)']_{UF}}} \quad (33)$$

The effect of reservoir length, x_1, on the dimensionless reciprocal rate derivative curve is illustrated in Figure 15. A unified dimensionless response is presented in Figure 16, from which the following governing equation is derived for the undefined flow, UF, regime with a slope of 0.33:

$$[t_D*(1/q_D)']_{UF} = 12782.64((t_D)_{UF}/x_1)^{0.33} \quad (34)$$

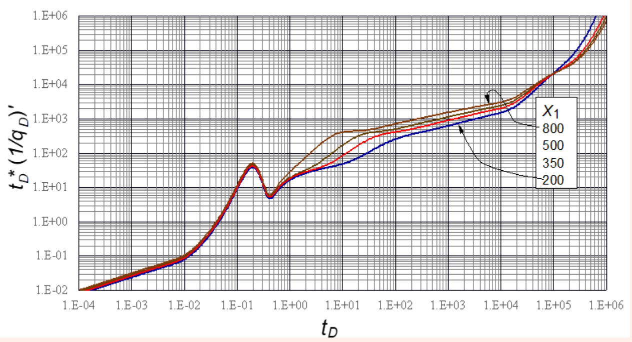

Figure 15: Effect of the reservoir length (x_1) on the dimensionless reciprocal rate derivative versus dimensionless time.

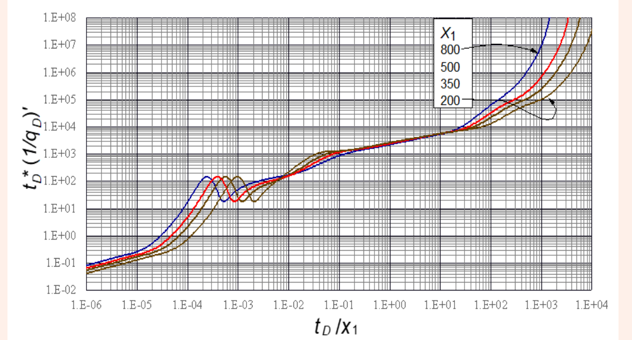

Figure 16: Unified behavior of the dimensionless reciprocal rate derivative versus dimensionless time for different reservoir lengths.

By substituting in Equation (34) the dimensionless time from Equation (3) and the dimensionless reciprocal rate derivative from Equation (7), and solving for x_1, the following expression is obtained:

$$x_1 = \left(\frac{23911.5\mu^{0.67} B t_{UF}^{0.33}}{(\phi c_t x_f^2)^{0.33} k^{0.67} h \Delta P [t*(1/q)']_{UF}}\right)^{1/0.33} \quad (35)$$

As expected, reservoir length and width do not influence the transient flow regimes; however, they do affect the late-time pseudosteady-state period. Figure 17 shows the impact of reservoir width (y_2) on the dimensionless reciprocal rate derivative curve, while Figure 18 presents the unified behavior from which the following governing equation is derived for the late pseudosteady-state period:

$$y_2 = [t_D * (1/q_D)']_{LP} = 1761.30[(t_D)_{LP}/y_2^{1.4}] \quad (36)$$

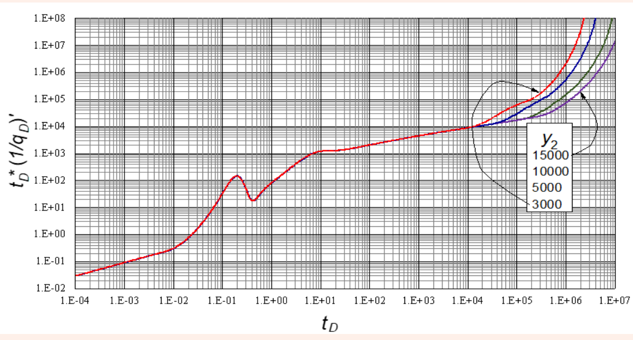

Figure 17: Effect of the reservoir width (y_2) on the dimensionless reciprocal rate derivative versus dimensionless time.

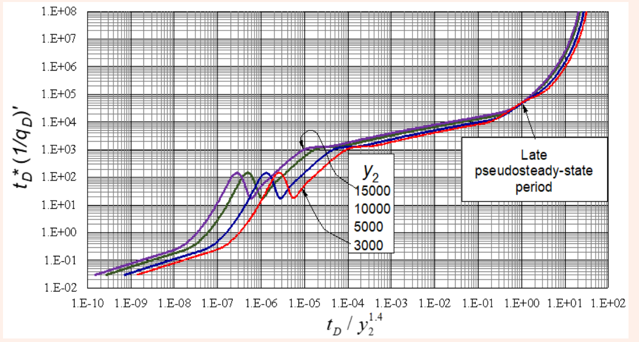

Figure 18: Unified behavior of the dimensionless reciprocal rate derivative versus dimensionless time for different reservoir widths.

Inserting the dimensionless time defined by Equation (3) and the dimensionless reciprocal rate derivative given in Equation (7) into Equation (36), and solving for y_2, leads to the following expression:

$$y_2 = \frac{208.161(B t_{LP})^{5/7}}{\{(c_t h \Delta P \phi)[t*(1/q)']_{LP}\}^{5/7} x_f^{10/7}} \quad (37)$$

During a transient rate test, both the reciprocal rate and its derivative exhibit exponential growth at late times, once the pseudosteady-state period is established. These two curves intersect at a unique point that is dependent on the reservoir size, specifically the reservoir length. Figure 19 illustrates the unified behavior of these responses and highlights the location of their intersection point. The coordinates of the intersection point are:

$$[t_D * (1/q)_D' x_1^{0.2}]_i = 667000 \quad (38)$$

$$[t_D * x_1^{0.5}]_i = 5210000 \quad (39)$$

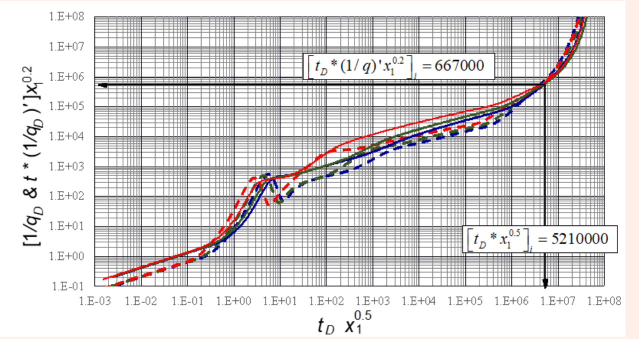

Figure 19: Unified dimensionless reciprocal rate and reciprocal rate derivative displaying the intersecting point between the two curves.

Substituting Equation (7) into (38) and Equation (3) into (39), and solving each for the reservoir width, yields the following results:

$$x_1 = \left(\frac{9.46\times10^7 \mu B}{kh\Delta P[t*(1/q)']_i}\right)^5 \quad (40)$$

$$x_1 = \left(\frac{19757299962.08\phi\mu c_t x_f^2}{k t_i}\right)^5 \quad (41)$$

The intersection of the various straight lines provides a means to solve for key reservoir parameters. For example, the intersection between Equations (28) and (30) results in the following relationship:

$$0.0278(t_D)_{ELIPi}/k = 6.299\sqrt{(t_D)_{ELIPi}/k} \quad (42)$$

$$x_f = \frac{1}{439.847}\sqrt{\frac{t_{ELIPi}}{\phi \mu c_t}} \quad (43)$$

The intersection between Equations (29) and (30) leads to:

$$0.0278(t_D)_{IPUFi}/k = 5913.62[(t_D)_{UF}/k]^{0.3} \quad (44)$$

Replacing the dimensionless time, Equation (3) in Equation (44) allows to obtain:

$$x_f = \frac{1}{6391.13}\sqrt{\frac{t_{IPUFi}}{\phi \mu c_t}} \quad (45)$$

The intersection between Equations (30) and (36) provides the following expressions:

$$1761.30[(t_D)_{UFLPi}/y_2^{1.4}] = 5913.62[(t_D)_{UFLPi}/k]^{0.3} \quad (46)$$

After plugging Equation (3) in Equation (46) the following relationship is obtained:

$$y_2 = 2.37536\sqrt{\frac{k t_{UFLPi}}{\phi \mu c_t x_f^2}} \quad (47)$$

Appendix A presents the required equations for straight-line conventional analysis in both pressure and rate transient analysis.

Examples

Although numerous examples were executed, only two are presented here for illustrative purposes.

Example 1

A simulated test in a multi-fractured horizontal well (MFHW) is provided in Figure 20. The following information was provided for simulation input. It is required to estimate the half-fracture length:

μ = 0.70 cp	B = 1.35 rb/STB	φ = 0.05	h = 100 ft
ct = 1x10-6 psi-1	q = 350 BPD	xf = 100 ft	

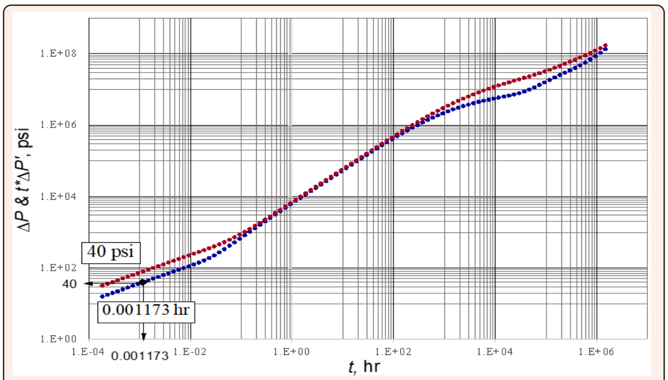

Figure 20: Pressure and pressure derivative versus time log-log plot for example 1.

The following arbitrary point was read from Figure 20:

tEL = 0.00117 hr (t*ΔP')EL = 40 psi

The half-fracture length is found using Equation (9):

$$x_f = \sqrt{\frac{42.3645(0.70)(350)^2(1.35)^2(1.17\times10^{-3})}{(0.05)(1\times10^{-6})(100)^2(40^2)}} = 98.36 \text{ ft}$$

Example 2

Another simulated test in a Multi-Fractured Horizontal Well (MFHW) was performed with the below information and provided in Figure 21. It is required to estimate the reservoir length:

μ = 0.70 cp	B = 1.35 rb/STB	φ = 0.05	h = 100 ft	x1 = 200 ft
ct = 1x10-6 psi-1	q = 350 BPD	k = 1 md	xf = 100 ft	

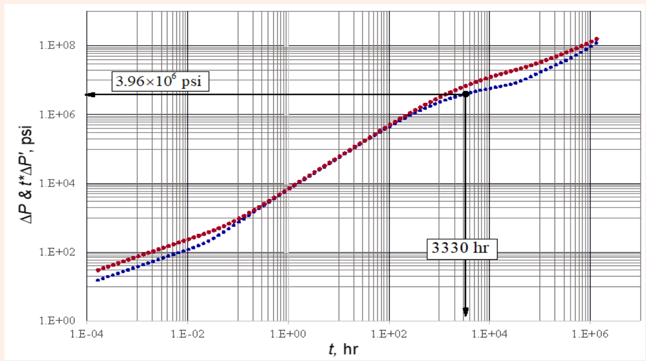

Figure 21: Pressure and pressure derivative versus time log-log plot for example 2.

The following arbitrary point was read from Figure 21:

t_{TL} = 3330 hr (t*ΔP')TL = 3960000 psi

The reservoir length, x_1, is estimated using Equation (21):

$$x_1 = \frac{30135435(0.70)(350)^2(1.35)^2(3330)}{(0.05)(1\times10^{-6})(1)(100)^2(100)^2(3.96\times10^6)^2} = 199.83 \text{ ft}$$

Comments on the Results

The application of the derived equations was validated through two representative examples. In the first case, the estimated half-fracture length (x_f) was 98.36 ft, compared to the actual input value of 100 ft used in the numerical simulation. This represents a relative error of only 1.64%, indicating a high degree of accuracy in the predictive capability of the proposed methodology.

In the second example, the calculated reservoir length (x_1) was 199.83 ft, in excellent agreement with the true input value of 200 ft. The minimal deviation (0.085%) further confirms the robustness and precision of the approach, particularly for identifying reservoir geometries under the assumed flow regimes. These results demonstrate that the derived analytical expressions are not only theoretically sound but also practically reliable when applied to synthetic test cases, providing confidence in their applicability to field data interpretation.

Conclusion

a. The application of the TDS methodology enabled the development of a robust analytical approach for interpreting pressure and reciprocal rate tests in Multi-Fractured Horizontal Wells (MFHW). By adopting the five-region model proposed by Molina & Zeidouni [4], the reservoir behavior could be decomposed into distinct flow regimes, offering a more detailed understanding of production dynamics and the interaction between the matrix and the fractures. Also, equations for conventional analysis are provided for both pressure and rate transient analysis.

b. The analysis of pressure derivative and reciprocal rate derivative plots allowed for the identification of characteristic lines and key transition points associated with various flow regimes, including early linear flow, intermediate pseudosteady-state, transitional linear flow, and late-time pseudosteady-state behavior, as well as the influence of the permeability modulus. This identification is critical to improving the accuracy of transient test interpretation and optimizing reservoir development strategies.

c. From the theoretical analysis, specific analytical expressions were derived to estimate key reservoir parameters such as the half-fracture length (x_f), the reservoir length (x_1), and the effective permeability. These equations provide a solid theoretical foundation for interpreting transient pressure and flow data in multifractured systems and represent a significant contribution to the TDS methodology.

d. However, the analysis of the dimensionless permeability modulus did not yield a fully unified behavior on the pressure derivative plot. This limitation suggests that further refinement is needed. Future research is recommended to improve the treatment of this parameter, possibly by incorporating additional scaling factors or alternative normalization approaches to enhance the grouping of responses and facilitate its practical application.

e. The validity of the derived expressions was confirmed through two synthetic examples. In the first case, the estimated half-fracture length was 98.36 ft, compared to the actual input value of 100 ft, resulting in a relative error of only 1.64%. In the second example, the calculated reservoir length was 199.83 ft, versus the true value of 200 ft, with an error below 0.1%. These results demonstrate the accuracy and reliability of the proposed analytical approach.

f. Overall, the TDS methodology applied to the five-region model proves to be an effective tool for interpreting pressure and flow behavior in multi-fractured horizontal wells. Its implementation can significantly contribute to the design of more efficient strategies for hydrocarbon recovery in unconventional reservoirs.

References

1. Clarkson CR, Qanbari F, Behmanesh H, Williams-Kovacs JD (2015) An approximate analytical multi-phase forecasting method for multi-fractured light tight oil wells with complex fracture geometry. Unconventional Resources Technology Conference (URTEC), USA.
2. Molina OM (2019) Application of pressure and rate transient analyses to stress-sensitive multi-fractured composite systems and compartmentalized reservoirs [PhD Dissertation]. Louisiana State University, USA.
3. Stalgorova E, Mattar L (2016) Analytical methods for single-phase oil flow: accounting for changing liquid and rock properties. SPE Europec featured at 78th EAGE Conference and Exhibition.
4. Molina O, Zeidouni M (2017) An enhanced nonlinear analytical model for unconventional multifractured systems. D031S007R006.
5. Tiab D (2005) Analysis of pressure derivative data of hydraulically fractured wells by the Tiab's Direct Synthesis technique. Journal of Petroleum Science and Engineering 49(1-2): 1-21.
6. Bernal KM, Escobar FH, Ghisays-Ruiz A (2014) Pressure and pressure derivative analysis for hydraulically-fractured shale formations using the concept of induced permeability field. Journal of Engineering and Applied Sciences 9(10): 1952-1958.
7. Escobar FH, Bernal KM, Olaya-Marin G (2014) Pressure and pressure derivative analysis for fractured horizontal wells in unconventional shale reservoirs using dual-porosity models in the stimulated reservoir volume. Journal of Engineering and Applied Sciences 9(12): 2650-2669.
8. Escobar FH, Rojas JD, Ghisays-Ruiz A (2015) Transient-rate analysis for hydraulically-fractured horizontal wells in naturally-fractured shale gas reservoirs. Journal of Engineering and Applied Sciences 10(1): 102-114.
9. Escobar FH, Montenegro LM, Bernal KM (2014) Transient-rate analysis for hydraulically-fractured gas shale wells using the concept of induced permeability field. Journal of Engineering and Applied Sciences 9(8): 1244-1254.
10. Pedrosa OA (1986) Pressure transient response in stress-sensitive formations. SPE-15115-MS.

Nomenclature

B	Oil reservoir volume, rb/STB
ct	System compressibility, 1/psi
h	Reservoir thickness, ft
k	Reservoir permeability, md
ki	Initial reservoir permeability, md
P	Pressure, psi
q	Rate, BPD
r	Radius , ft
SRV	Stimulated reservoir volume
t	Time, hr
tD	Dimensionless time
tD*PD'	Dimensionless pressure derivative
t*ΔP'	Pressure derivative, psi
tD*(1/qD)'	Dimensionless reciprocal rate derivative
t*(1/q)'	Reciprocal rate derivative, 1/BPD
xf	Half-fracture length, ft
x1	Region 2 length, ft
x1	Region 2 + region 3 length, ft
y2	Reservoir width, ft
wf	Fracture width, ft
1/q	Reciprocal rate, 1/BPD

Suffices

D	Dimensionless, Dimension
EL	Early linear
ELIPi	Intercept between early linear and intermediate pseudosteady state
ELLPi	Intercept between early linear and late pseudosteady state
i	Intercept of reciprocal rate and reciprocal rate derivative
IP	Intermediate pseudosteady-state period
IPTLi	Intercept between intermediate pseudosteady state and transitory linear
IPUFi	Intercept between intermediate pseudosteady state and undefined flow
TL	Transitory linear flow regime
UF	Undefined flow regime
UFLPi	Intercept between undefined flow and late pseudosteady state
v	Vertical

Greek

Δ	Change, drop
φ	Porosity, fraction
γ	Reservoir permeability modulus, psi
μ	Viscosity, cp

Appendix A

From a Cartesian plot of ΔP versus t0.5, equation (8) will yield an equation to estimate the half-fracture length:

$$x_f = \sqrt{\frac{29.8484 q\mu B}{h m_{EL}} \sqrt{\frac{1}{\phi \mu c_t}}} \quad (A.1)$$

From a Cartesian plot of ΔP versus t, equation (10) will yield:

$$x_f = \sqrt{\frac{0.02396 qB}{h m_{IP} \phi c_t}} \quad (A.2)$$

From a Cartesian plot of ΔP versus $t^{0.5}$, equation (12) will yield:

$$x_f = \sqrt{\frac{0.02396 qB}{h m_{IP} \phi c_t}} \quad (A.3)$$

From a Cartesian plot of ΔP versus $t^{0.5}$, equation (20) will yield:

$$x_1 = \left(\frac{25174.3395 q\mu B}{h m_{TL} k^{0.5}} \sqrt{\frac{1}{\phi \mu c_t x_f^2}}\right)^{\frac{1}{0.5}} \quad (A.4)$$

From a Cartesian plot of ΔP versus t, equation (22) will yield:

$$y_2 = \frac{1.4711 qB}{h m_{LP} \phi c_t x_f^2} \quad (A.5)$$

From a Cartesian plot of $1/q_D$ versus $t^{0.5}$, equation (28) will yield:

$$k = \sqrt{\frac{12.8863 q\mu B}{h m_{EL}} \sqrt{\frac{1}{\phi \mu c_t x_f^2}}} \quad (A.6)$$

From a Cartesian plot of $1/q_D$ versus t, equation (29) will yield:

$$k = \left(\frac{0.001035 q\mu B}{h m_{IP}} \sqrt{\frac{1}{\phi \mu c_t x_f^2}} \right)^{\frac{2}{5}} \quad (A.7)$$

From a Cartesian plot of $1/q_D$ versus $t^{0.3}$, equation (30) will yield:

$$k = \left(\frac{234909.128 q\mu B}{h m_{UF}} \sqrt{\frac{1}{\phi \mu c_t x_f^2}} \right)^{\frac{5}{9}} \quad (A.8)$$

From a Cartesian plot of $1/q_D$ versus $t^{0.33}$, equation (34) will yield:

$$x_1 = \left(\frac{3605019825 q\mu B}{h m_{UF} k^{0.67}} \left(\frac{1}{\phi \mu c_t x_f^2} \right)^{0.33} \right)^{\frac{1}{0.33}} \quad (A.9)$$

From a Cartesian plot of $1/q_D$ versus t, equation (36) will yield:

$$y_2 = \left(\frac{65.5810 q\mu B}{h m_{LP} k^{0.5}} \sqrt{\frac{1}{\phi \mu c_t x_f^2}} \right)^{\frac{5}{7}} \quad (A.10)$$